GLOBAL BIOGEOCHEMICAL CYCLES, VOL. 13, NO 2, PAGES 679-694, JUNE 1999

Mathematical modeling of nitrous oxide emissions from an agricultural field during spring thaw

R.F. Grant
Department of Renewable Resources, University of Alberta, Edmonton, Alberta, Canada

E. Pattey
Eastern Cereal and Oilseeds Research Centre, Ottawa, Ontario, Canada

Abstract. Confidence in regional estimates of N_2O emissions used in national greenhouse gas inventories could be improved by using mathematical models of the biological and physical processes by which these emissions are known to be controlled. However these models must first be rigorously tested against field measurements of N_2O fluxes under well documented site conditions. Spring thaw is an active period of N_2O emission in northern ecosystems and thus presents conditions well suited to model testing. The mathematical model *ecosys*, in which the biological and physical processes that control N_2O emissions are explicitly represented, was tested against N_2O and CO_2 fluxes measured continuously during winter and spring thaw using gradient and eddy covariance techniques. In the model, ice formation at the soil surface constrained soil-atmosphere gas exchange during the winter, causing low soil O_2 concentrations and consequent accumulation of denitrification products in the soil profile. The removal of this constraint to gas exchange during spring thaw caused episodic emissions of N_2O and CO_2, the timing and intensities of which were similar to those measured in the field. Temporal variation in these emissions, both simulated and measured, was high, with those of N_2O ranging from near zero to as much as 0.8 mg N m^{-2} h^{-1} within a few hours. Such variation should be accounted for in ecosystem models used for temporal integration of N_2O fluxes when making long-term estimates of N_2O emissions.

1. Introduction

Techniques for estimating emissions of N_2O from soils are needed to evaluate management options for reducing such emissions as part of the Canadian commitment to reduce the greenhouse gases released to the atmosphere. However N_2O emissions are controlled by several interacting soil attributes, including temperature [*Bremner and Shaw*, 1958; *Nommik*, 1956], O_2 [*Allison et al.*, 1960], NO_3^- and organic matter [*Smid and Beauchamp*, 1976], such that temporal and spatial profiles of emissions under site-specific conditions are complex. Consequently, the predictive value of short term measurements for long term estimates of N_2O emissions is confined to sites with similar soil and climate [*Blackmer et al.*, 1982].

Long-term estimates of N_2O emissions may be made through mathematical modeling of processes such as nitrification and denitrification from which emissions occur. These emissions have been represented in models by functions of NO_3^- and available carbon which are modified by dimensionless factors for soil water content and temperature [*Li et al.*, 1992; *Parton et al.*, 1996]. However short term temporal variation in N_2O emissions is too large to be explained from simple functions of soil water content, temperature, or N and C substrates [*Blackmer et al.*, 1982; *Christensen*, 1983; *Flessa et al.*, 1995; *Robertson*, 1994), indicating that N_2O fluxes are determined by complex interactions among N transformation and transport processes and the environmental conditions under which they function. Such interactions need to be more fully represented in these models if they are to simulate N_2O fluxes reliably. Therefore the kinetics of the NH_4^+ oxidation and the NO_3^- reduction pathways, which have been simulated under controlled laboratory conditions [*Grant*, 1994; *Leffelaar and Wessel*, 1988; *McConnaughey and Bouldin*, 1985], must be linked to simulations of water, heat and O_2 transfer if they are to be used to estimate N_2O emissions under field conditions. This linkage is especially important in the estimation of emissions from denitrification during spring thaw when transfer processes are affected by phase changes of water.

The dissimilatory reduction of NO_3^- is understood to proceed through a sequence of reaction products that include NO_2^-, NO^-, N_2O and N_2, the last three of which may be emitted as gases. The reduction of NO_3^- is suppressed by O_2, and reduction of N_2O is suppressed by NO_3^- [*Blackmer and Bremner*, 1978; *Firestone et al.*, 1979; *Weier et al.*, 1993]. These reaction kinetics suggest a declining preference for electron acceptors of $O_2 > NO_3^- > NO_2^- > N_2O$ by the facultative anaerobes responsible for denitrification [*Cady and Bartholomew*, 1961]. A direct inhibition by NO_3^- on N_2O reduction has been used in some models to simulate denitrification reaction sequences [*Arah and Vinten*, 1995; *McConnaughey and Bouldin*, 1985], although such inhibition has

Paper number 1998GB900018.
0886-6236/99/1998GB900018$12.00

not been observed experimentally [*Betlach*, 1979]. We hypothesize that the above preference scheme without inhibition effects, coupled to a transport scheme for heat, water, O_2 and solutes, can explain soil N_2O emissions during spring thaw. This preference scheme for electron acceptors has been used to simulate temporal changes in denitrification reaction products and their ratios under laboratory conditions [*Grant et al.*, 1993c] and in N_2O emissions under field conditions [*Grant et al.*, 1993d] when coupled to heat, water and O_2 transport algorithms [*Grant*, 1992; *Grant et al.*, 1995] as part of the ecosystem model *ecosys* [*Grant*, 1996]. Although the model has reproduced the flush in N_2O emissions commonly observed in northern ecosystems following snowmelt, the extent to which simulated emissions could be tested with measured data was constrained by limitations in the measurement techniques available at the time.

Recent developments in tunable diode laser instrumentation [*Ogram et al.*, 1988; *Wagner-Riddle et al.*, 1996] and in micrometeorological techniques for measuring N_2O emissions [*Wienhold et al.*, 1994] provide opportunities for more detailed testing of our hypothesis than were previously available. Such testing is necessary to establish confidence in model estimates of short and long term emissions that are based on the hypothesis. Here we report results from tests of the ecosystem simulation model *ecosys*, in which the dissimilatory reduction sequences of both nitrification [*Grant*, 1995] and denitrification [*Grant et al.*, 1993c,d] are explicitly represented, with micrometeorological measurements of N_2O emissions from an agricultural field during winter and early spring.

2. Model Development

2.1. General

The preference scheme for electron acceptors is part of the model of C, N and P transformations described by *Grant et al.* [1993a,b]. This model is based on five organic states among which C, N and P may move: solid organic matter (S), soluble organic matter (P), sorbed organic matter (B), microbial communities (M), and microbial residues (Z). Each state is resolved into between two and four hierarchical levels of biological organization, listed below in decreasing order, for which the descriptors *i*, *n*, *j* and *k* are used:

i organic matter-microbe complex;
n functional type within each complex (microbial populations only);
j structural or kinetic components within each complex or functional type;
k elemental fraction within each component.

These levels are shown in greater detail in Table 1. Thus the solid organic matter (S) in each soil layer is represented in each of four independent organic matter-microbe complexes S_i, where *i* is animal manure, plant residue, active soil organic matter, or passive soil organic matter. Each S_i is further resolved into kinetic components $S_{i,j}$ each of which is assumed to be a homogeneous substrate of differing resistance to microbial decomposition. For example, S_y (where *y* is plant residue) is resolved into components of protein, carbohydrate, cellulose, and lignin. Each component consists of elemental fractions $S_{i,j,k}$, where *k* is carbon , nitrogen or phosphorus. Each S_i is associated with a heterotrophic microbial community M_i, resolved into functional types $M_{i,h}$, where *h* is obligately aerobic bacteria [*Grant et al.*,1993a,b], facultatively anaerobic denitrifiers [*Grant et al.*, 1993c,d], fungi, anaerobic fermenters plus H_2-producing acetogens [*Grant*, 1998] and acetotrophic methanogens [*Grant*, 1998]. There is also an autotrophic microbial community that includes NH_4^+ and NO_2^- oxidizers [*Grant*, 1994, 1995], CH_4 oxidizers (*Grant*, 1999) and hydrogenotrophic methanogens [*Grant*, 1998]. Each $M_{i,h}$ has structural components $M_{i,h,j}$, where *j* is labile, resistant, or storage. The labile component is used to divide each $M_{i,h}$ into active *a* or quiescent *q* kinetic components from which the specific activity of each population is calculated [*Grant et al.*, 1993a]. Each $M_{i,h,j}$ consists of fractions $M_{i,h,j,k}$ where *k* is carbon, nitrogen or phosphorus. A general flow diagram for the transformation of material in the soil ecosystem is given in Figs. 1 and 2 of *Grant et al.* [1993a].

The model functions in one, two or three dimensions by representing all state and rate variables according to their north-south *x*, east-west *y* and vertical *z* positions within a complex landscape. This is accomplished by adding three descriptors for landscape position to those for biological organization described above. Thus the solid organic matter variable $S_{i,j,k}$ would be represented at the landscape level as $S_{x,y,z,i,j,k}$. The landscape descriptors are omitted here for clarity.

2.2. C oxidation and O_2 Reduction

The microbially driven decomposition of the solid organic substrates $S_{i,j}$ in *ecosys* [*Grant et al.*, 1993a equations (1) – (7)] causes decomposition products to accumulate in soluble pools P_i. The oxidation of $P_{i,c}$ by heterotrophs during respiration creates a demand for electron acceptors:

$$R'_{i,h} = \{R'_h M_{i,h,a} [P_{i,c}]/(K_{Rh} + [P_{i,c}])\} f_t f_w \quad (1)$$

Definitions of model variables are given in the notation section and values of input parameters are given in Table 2. The value of f_t is calculated from soil temperature [*Grant et al.*, 1995] as shown by *Grant et al.* [1993a equation (5)]. The value of f_w is calculated from soil water potential [*Grant*, 1992] based on the functions of *McGill et al.* [1981] and *Pirt* [1975]. Results from testing f_t and f_w are given by *Grant and Rochette* [1994].

The demand for electron acceptors created by $R'_{i,h}$ in (1) may be partially met by O_2:

$$R_{o_2 i,h} = 4\pi\, n\, M_{i,h,a}\, D_{S_{O_2}} (d_m\, d_w/(d_w - d_m)) ([O_{2S}] - [O_{2m}]) \quad (2a)$$

$$R_{o_2 i,h} = R'_{o_2 i,h} [O_{2m}]/([O_{2m}] + K_{o_2 h}) \quad (2b)$$

Oxygen uptake rate $R_{o_2 i,h}$ is solved from a convergence solution for the O_2 concentration at microbial microsites $[O_{2m}]$ at which O_2 diffusion through the soil solution (equation (2a)) equals O_2 uptake at microbial microsites (equation (2b)). The diffusion path length is the effective water film thickness calculated from soil water potential according to *Kemper and Rollins* [1966]. The concentration of O_2 in the soil solution $[O_{2S}]$ that drives diffusion is calculated from convective-dispersive transport of O_2 in aqueous and gaseous phases and from volatilization-dissolution transfer of O_2 between aqueous and gaseous phases as described in (14) – (21) below. The convergence solution for O_2 uptake by each aerobic population in the model is constrained by total O_2 uptake of all aerobic populations, thereby simulating competition for O_2 uptake among aerobic populations. The microbial demand for O_2 uptake $R'_{o_2 i,h}$ is equal to 2.67 $R'_{i,h}$ from (1) given that C

Table 1. Levels of Biological Organization at Which Each Organic State is Represented in *Ecosys*.[¶]

Organic State	Substrate - Microbe Complex *i*	Functional Type (Microbes) *n*	Structural or Kinetic Component *j*	Elemental Fraction *k*
Solid Organic Matter (S)	animal manure plant residue active OM passive OM		protein carbohydrate cellulose lignin	carbon nitrogen phosphorus
Soluble Organic Matter (P)	animal manure plant residue active OM passive OM			carbon nitrogen phosphorus
Acetate (A)	animal manure plant residue active OM passive OM			carbon
Sorbed Organic Matter (B)	animal manure plant residue active OM passive OM			carbon nitrogen phosphorus
Microbial Communities (Heterotrophic) (M)	animal manure plant residue active OM passive OM	aerobic bacteria denitrifiers fungi fermenters + acetogens acetotrophic methanogens	labile resistant storage	carbon nitrogen phosphorus
Microbial Communities (Autotrophic) (M)		NH_4^+ oxidizers NO_3^- oxidizers methanotrophs hydrogenotrophic methanogens	labile resistant storage	carbon nitrogen phosphorus
Microbial Residues (Z)	animal manure plant residue active OM passive OM		labile resistant	carbon nitrogen phosphorus

[¶] Levels are in decreasing order from left to right.

donates 4 mol e^- mol^{-1} C during oxidation and that O_2 accepts 4 mol e^- mol^{-1} O_2 during reduction.

2.3. N Reduction

The demand for electron acceptors unmet by O_2 creates a demand from heterotrophic denitrifiers ($h = d$) for other acceptors:

$$R_e = 0.125 f_e (R'_{O_2}i,d - R_{O_2}i,d) \quad (3)$$

given that O_2 accepts 4 mol e^- mol^{-1} O_2 (= 0.125 mol e^- g^{-1} O_2). The value selected for f_e in Table 2 is based on the finding of *Koike and Hattori* [1975a] that denitrifier growth rates under anaerobic conditions are 1/5 to 1/7 of those under aerobic conditions. The unmet demand for electron acceptors may be transferred sequentially to NO_3^-, NO_2^- and N_2O:

$$R_{NO_3}i,d = 7 R_e [NO_3^-]/([NO_3^-] + K_{NO_3}d) \quad (4)$$

$$R_{NO_2}i,d = (7 R_e - R_{NO_3}i,d) [NO_2^-]/([NO_2^-] + K_{NO_2}d) \quad (5)$$

$$R_{N_2O}i,d = 2 (7 R_e - R_{NO_3}i,d - R_{NO_2}i,d) [N_2O]/([N_2O] + K_{N_2O}d) \quad (6)$$

given that NO_3^- and NO_2^- accept 2 mol e^- mol^{-1} N (= 7 g N mol^{-1} e^-) and that N_2O accepts 1 mol e^- mol^{-1} N (= 14 g N mol^{-1} e^-) during reduction. This transfer scheme is similar to that proposed by *Ameida et al.* [1995] to explain competition between NO_3^- and NO_2^- reduction during denitrification. Under aerobic conditions $[O_2m] >> K_{O_2}h$ and hence $R_{O_2}i,d \rightarrow R'_{O_2}i,d$ (equation (2)) so that R_e (equation (3)) and hence $R_{NO_3}i,d$ (equation (4)) is small. Similarly if $[NO_3^-] >> K_{NO_3}d$ then $R_{NO_3}i,d \rightarrow 7 R_e$ (equation (4)) so that $R_{NO_2}i,d$ is small (equation (5)), and if $[NO_2^-] >> K_{NO_2}d$ then $R_{NO_2}i,d \rightarrow 7 R_e - R_{NO_3}i,d$ (equation (5)) so that $R_{N_2O}i,d$ is small (equation (6)). In this way the model supresses the reduction of less preferred electron acceptors in the presence of more preferred ones.

2.4. Microbial Growth

The oxidation of C (equation (1)) is coupled to the reduction of O_2 (equation (2)) by all heterotrophs:

Table 2. Values of Parameters Required in the Modeling of N_2O[¶]

Parameter	Equation	Value	Source
$D_{g_{N_2O}}$	(18)	5.6×10^{-2} m^2 h^{-1}	
$D_{s_{N_2O}}$	(16)	5.7×10^{-6} m^2 h^{-1}	
d_m	(2)	10^{-6} m	
f_e	(3)	0.25	*Koike and Hattori* [1975a]
ΔG_d	(12)	-10 kJ g C^{-1}	*Koike and Hattori* [1975a]
$\Delta G_{h(h=d)}$	(12)	-25 kJ g C^{-1}	*Koike and Hattori* [1975a]
G_M	(12)	25 kJ g C^{-1}	
$K_{NO_2 d}$	(5)	10.0 g N m^{-3}	*Yoshinari et al.* [1977]
$K_{NO_3 d}$	(4)	10.0 g M m^{-3}	*Yoshinari et al.* [1977]
$K_{N_2O d}$	(6)	1.0 g N m^{-3}	*Yoshinari et al.* [1977]
$K_{O_2 h}$	(2)	0.032 O_2 g m^{-3}	*Griffin* [1972]
$K_{R h}$	(1)	35g C m^{-3}	*McGill et al.* [1981]
n	(2)	2.4×10^{12} g^{-1}	
R'_h	(1)	0.2 g C g C^{-1}h^{-1}	*Ridge* [1976] and *Shields et al.* [1974]
S_{N_2O}	(14)	0.524	*Wilhelm et al.* [1977]

[¶] see equations (1) – (20) in text

$$R_{i,h} = R'_{i,h} R_{O_2 i,h} / R'_{O_2 i,h} \quad (7)$$

where the term $R_{O_2 i,h} / R'_{O_2 i,h}$ represents O_2 constraints to C oxidation calculated in (2). Additional oxidation of C by denitrifiers ($h = d$) is coupled to the reduction of NO_3^-, NO_2^- and N_2O:

$$R_{i,d} = 0.429 R_{NO_3 i,d} + 0.429 R_{NO_2 i,d} + 0.214 R_{N_2O i,d} \quad (8)$$

given that C donates 4 mol e^- mol C^{-1} during oxidation and that NO_3^- and NO_2^- accept 2 mol e^- mol N^{-1} and N_2O accepts 1 mol e^- mol N^{-1} during reduction. Total oxidation of C by denitrifiers is therefore

$$R_i = R_{i,h} + R_{i,d} \quad (9)$$

C oxidation by obligate aerobes (equation (7)) and facultative denitrifiers (equation (9)) drives maintenance respiration [*Grant et al.*, 1993a equations (18) and (19)] and growth respiration, calculated as the difference between C oxidation and maintenance respiration. The energy yields from aerobic and denitrifier growth respiration drive the uptake of additional decomposition products and their transformation into microbial biomass so that total uptake of decomposition products by obligate aerobes is

$$U_{i,h,c} = R_{Mi,h} + (R_{i,h} - R_{Mi,h})(1.0 + Y_h) \quad [R_{i,h} > R_{Mi,h}] \quad (10a)$$

$$U_{i,h,c} = R_{i,h} \quad [R_{i,h} < R_{Mi,h}] \quad (10b)$$

and by facultative denitrifiers is

$$U_{i,h(h=d),c} = R_{Mi,h} + (R_{i,h} - R_{Mi,h})(1.0 + Y_h) + R_{i,d}(1.0 + Y_d) \quad [R_{i,h} > R_{Mi,h}] \quad (11a)$$

$$U_{i,h(h=d),c} = R_{i,h} + R_{i,d}(1.0 + Y_d) \quad [R_{i,h} < R_{Mi,h}] \quad (11b)$$

The energy yields Y_h and Y_d are calculated by dividing the free energy change of the oxidation-reduction reactions by the energy required to construct new microbial biomass from decomposition products:

$$Y_h = -\Delta G_h / G_M \quad (12a)$$

$$Y_d = -\Delta G_d / G_M \quad (12b)$$

Neglecting maintenance respiration, growth yield may be calculated from ΔG as $(U_{i,h} - R_{i,h})/U_{i,h} = Y/(1 + Y)$ (equations (10) – (12)). Values for ΔG_h and ΔG_d of -25 and -10 kJ g C^{-1} respectively used in *ecosys* for facultative anaerobes (Table 2) thus give growth yields of (25/25)/(1 + 25/25) = 0.5 and (10/25)/(1 + 10/25) = 0.3 mol C mol C^{-1} for reduction of O_2 and N oxides respectively. The model growth yield for O_2 reduction is consistent with values reported by *McGill et al.* [1981], and the energy yield of denitrification has been reported to be about one half that of O_2 reduction [*Elliott and Gilmour*, 1971]. The use of the same value of ΔG_d for all denitrifier reductions is based on the observation by *Koike and Hattori* [1975b] that the energy yield from the reduction to N_2 of NO_3^-, NO_2^- and N_2O is proportional to the oxidation state of the reductant.

Net growth of each heterotrophic population is calculated as total uptake of substrate decomposition products minus C oxidation for maintenance and growth respiration and for decomposition of each microbial structural component j:

$$\delta M_{i,h,j,c}/\delta t = F_j U_{i,h,c} - F_j R_{i,h} - D_{i,h,j,c} \quad [R_{i,h} > R_{Mi,h}] \quad (13a)$$

$$\delta M_{i,h,j,c}/\delta t = F_j U_{i,h,c} - R_{Mi,h,j} - D_{i,h,j,c} \quad [R_{i,h} < R_{Mi,h}] \quad (13b)$$

$$\delta M_{i,h,c}/\delta t = \sum_{j=1}^{J} \delta M_{i,h,j,c}/\delta t \quad (13c)$$

Growth of heterotrophs ($\delta M_{i,h,c}/\delta t$) requires the immobilization-mineralization of inorganic N and P which is calculated from microbial N:C and P:C ratios ($M_{i,h,n}$:$M_{i,h,c}$ and $M_{i,h,p}$:$M_{i,h,c}$ respectively) as given by *Grant et al.* [1993a equation (23)]. Decomposition of $M_{i,h,j,c}$ ($D_{i,h,j,c}$) is calculated from $M_{i,h,j,c}$ and soil temperature as given in *Grant et al.* [1993a equations (21) – (22)], and microbial decomposition products are partitioned into microbial residues $Z_{i,j,k}$ and soil organic matter

$S_{i,j,k}$ (where i is passive soil organic matter) as in *Grant et al.* [1993a equations (26) – (28)]. The time integral of $\delta M_{i,h,c}$ /δt from (13) gives heterotrophic biomass $M_{i,h,c}$ which is used to calculate active biomass $M_{i,h,a}$ [*Grant et al.*, 1993a equation (24)] from which C oxidation $R'_{i,h}$ is calculated in (1). Microbial populations are thus active agents of organic transformations in *ecosys*, rather than passive repositories of C, N and P as in most other ecosystem models.

2.5. Transport of Microbial Substrates and Products

All soluble substrates and products of microbial transformations (including $P_{i,k}$, CO_2, O_2, NO_3^-, NO_2^-, N_2O, N_2, NH_4^+ and $H_2PO_4^-$) undergo convective-dispersive transport through aqueous phases of the soil and root. Those substrates and products with a gaseous phase (CO_2, O_2, N_2O, N_2 and NH_3) also undergo volatilization-dissolution transfer between aqueous and gaseous phases, and convective-dispersive transport through gaseous phases of the soil and root. Transfer between gaseous and aqueous phases in the soil is calculated for each substrate or product γ as described by *Skopp* [1985]:

$$T_\gamma = A_{gs} D_{t_\gamma} (S_\gamma f_{t_{gs\gamma}} [\gamma_g] - [\gamma_s]) \quad (14)$$

Transfer is thus driven by concentration differences between gaseous and aqueous phases in the soil. The value of A_{gs} in (14) is estimated from air-, water-, and ice-filled porosity [*Skopp*, 1985]. Gaseous solubilities are calculated from soil temperature [*Grant*, 1992; *Grant et al.*, 1995] and from the temperature-dependent solubility coefficients S_γ of *Wilhelm et al.* [1977]. Transfer between gaseous and aqueous phases in the root are calculated in the same way as those in the soil [*Grant*, 1993b].

Vertical transport between adjacent layers in the aqueous phase of the soil is calculated for each substrate or product γ as the sum of convective and dispersive-diffusive components:

$$Q_{s\gamma} = Q_w [\gamma_s] + D_{s\gamma} \Delta[\gamma_s]/\Delta z \quad (15)$$

The calculation of the vertical water flux Q_w in *ecosys* is described elsewhere [*Grant*, 1992; *Grant et al.*, 1995]. The value of the effective dispersion-diffusion coefficient $D_{s\gamma}$ is the geometric mean of the coefficients in each layer which are calculated according to Bresler (1973):

$$D_{s\gamma} = \lambda |Q_w| + D'_{s\gamma} f_{t_s} \tau_s \theta_s \upsilon_s \quad (16)$$

If the total gaseous equivalent concentration of aqueous gases γ exceeds that at atmospheric pressure, an upward flux equivalent to the excess partial pressure of each gas is added to $Q_{s\gamma}$.

Vertical transport between adjacent layers in the gaseous phase of the soil is calculated for each substrate or product γ with a gaseous phase as the sum of convective and diffusive components:

$$Q_{g\gamma} = -(Q_w + U_w) [\gamma_g] + D_{g\gamma} \Delta[\gamma_g]/\Delta z \quad (17)$$

The first term on the right hand side of (17) represents the vertical transport of soil air arising from vertical transport of water through soil and radial uptake of water by plant roots. The value of $D_{g\gamma}$ is the geometric mean of the diffusion coefficients in each layer which are calculated according to *Millington* [1959] with a temperature function from *Campbell*]1985]:

$$D_{g\gamma} = D'_{g\gamma} f_{t_g} \theta_g \upsilon_g / \theta_p^2 \quad (18)$$

Air-filled porosity θ_g in (18) is controlled by soil water and ice contents, values of which are calculated from a solution to the general heat flux equation [*Grant*, 1992; *Grant et al.*, 1995].

Vertical transport between the atmosphere and the aqueous phase of the soil surface layer is calculated for each substrate or product γ with a gaseous phase as

$$Q'_{s\gamma} = g_a \{[\gamma_a] - \{D_{s\gamma} [\gamma_s]/(0.5 \Delta z') + g_a [\gamma_a]\}/\{D_{s\gamma} S_\gamma f_{t_{gs\gamma}} /(0.5 \Delta z') + g_a\}\} \quad (19)$$

such that the gaseous transport of each γ between the atmosphere and the soil surface is equal to the aqueous transport between the soil surface and the midpoint of the uppermost soil layer (0.5 $\Delta z'$). Vertical transport between the atmosphere and the gaseous phase of the soil surface layer is calculated for each substrate or product γ with a gaseous phase as

$$Q'_{g\gamma} = g_a \{[\gamma_a] - \{D'_{g\gamma} [\gamma_g]/(0.5 \Delta z') + g_a [\gamma_a]\}/\{D'_{g\gamma}/(0.5 \Delta z') + g_a\}\} \quad (20)$$

such that the gaseous transport of each γ between the atmosphere and the soil surface is equal to the gaseous transport between the soil surface and the midpoint of the uppermost soil layer. Total surface flux is thus

$$Q'_\gamma = Q'_{s\gamma} + Q'_{g\gamma} \quad (21)$$

3. Model Testing

3.1 Laboratory Experiment

Results from the laboratory experiment of *Koike and Hattori* [1975a] were used to test values of growth yields Y_h and Y_d (equation (12)) under controlled conditions. In their experiment, *Koike and Hattori* [1975a] used a spectrophotometric technique to measure the growth of *Pseudomonas denitrificans* in aerobic versus anaerobic batch cultures at 30°C in which 5 mM glutamate was the sole source of C and energy.

This experiment was simulated by initializing *ecosys* with an inorganic, nonreactive soil in which only denitrifiers ($h = d$) were present. The model soil was amended with NO_3^-, $H_2PO_4^-$ and an amino acid residue [*Grant et al.*, 1993a] at the concentrations used by *Koike and Hattori* [1975a]. The model was then run under ambient and zero atmospheric O_2 concentrations at 30°C and high humidity (to prevent drying of the simulated soil). Model results for denitrifier growth yields were compared with those reported by *Koike and Hattori* [1975a].

3.2 Field Experiment

The field experiment was carried out from 25 February to 15 April 1996 over a flat 23 ha field of Dalhousie clay loam (Table 3) located in an open area surrounded by other flat fields at the Greenbelt Farm in Ottawa, Canada. Fluxes of momentum, CO_2, and of sensible and latent heat were calculated every 30 min. from air temperature, three-dimensional wind velocity (sonic anemometer DAT-310, Kaijo-Denki Company, Tokyo), and from H_2O and CO_2 molar fractions (infrared gas analyzer LI-6262, LI-COR Inc., Lincoln, Nebraska) recorded at 20 Hz and a height of 1.75 m with an eddy covariance system developed by *Pattey et al.* [1996]. At this height the estimated footprint [*Horst and Weil*, 1994] for integrating 90% of the flux ranges from 75 to 250 m

Table 3. Properties of the Dalhousie Clay Loam at the Greenbelt Farm Used in *Ecosys*.[¶]

	Depth, m							
	0.010	0.075	0.15	0.25	0.35	0.45	0.75	1.15
BD, Mg m^{-3}	1.31	1.31	1.31	1.31	1.31	1.31	1.40	1.40
θ_{FC}, m^3 m^{-3}	0.38	0.38	0.38	0.38	0.38	0.38	0.38	0.38
θ_{WP}, m^3 m^{-3}	0.22	0.22	0.22	0.22	0.22	0.22	0.22	0.22
K_{sat}, mm h^{-1}	6.3	6.3	6.3	6.3	6.3	6.3	6.3	6.3
Sand, g kg^{-1}	257	257	257	257	257	257	257	257
Silt, g kg^{-1}	417	417	417	417	417	417	417	417
*p*H	6.79	6.79	6.79	7.13	7.13	7.13	7.19	7.19
CEC, cmol kg^{-1}	25.5	25.5	25.5	25.5	25.5	25.5	24.5	23.5
Org. C, g kg^{-1}	30.7	30.7	30.7	4.7	4.7	4.7	2.0	2.0
Org. N, g Mg^{-1}	2560	2560	2560	390	390	390	165	165
NH_4^+, g Mg^{-1}*	0.00	0.00	0.00	0.00	0.00	0.00	0.00	0.00
NO_3^-, g Mg^{-1}*	31.36	31.36	31.36	5.64	5.64	5.64	4.88	4.88
θ, m^3 m^{-3}*	.235	.373	.376	.378	.378	.378	.378	.378

[¶] abreviations are as follows: BD, bulk density; θ , water content; K_{sat}, saturated hydraulic conductivity; and CEC, cation exchange capacity..

* initial values measured on 1 September 1995.

depending on atmospheric stability. Fluxes of N_2O and CO_2 were calculated every 30 min. from a gradient technique using a tunable laser diode trace gas analyzer (Campbell Scientific, Logan, Utah) with inlets at heights of 1.0 and 2.0 m. Fluxes were calculated from the following equations in which K is defined in the inertial sublayer [*Paulson*, 1970]:

$$Q'_\gamma = - k u_* (\gamma_{a_2} - \gamma_{a_1})/\{\alpha \{\ln[(z_2 - d)/(z_1 - d)] - \psi h_2 + \psi h_1\}\} \quad (22)$$

in which

$$\psi h = -5\ z/L \quad \text{for stable conditions} \quad (23)$$

$$\psi h = 2 \ln[(1 + x^2)/2] \text{ for unstable conditions } [x = (1 - 16\ z/L)^{1/4}] \quad (24)$$

where γ_{a_2} and γ_{a_1} are the atmospheric N_2O or CO_2 concentrations(g m^{-3}) measured at heights z_2 and z_1 (meters); k is the von Karman constant (0.4); u_* (m s^{-1}) is the friction velocity calculated from the momentum flux; L (meters) is the Monin-Obukov length calculated from the momentum and sensible heat fluxes, and α is the inverse of an enhancement factor required for measurements in the roughness sublayer (equal to 1 in the inertial sublayer). It is assumed that measurements were taken in the inertial sublayer and that the stability corrections for N_2O and CO_2 are similar to that for heat. A correction was introduced [see *Simpson et al.*, 1998] to account for the lack of energy budget closure over agricultural fields. Wind speeds are higher during winter than summer at this site, so that turbulent conditions were prevalent during the experiment.

Soil temperatures were measured continuously at half-hourly intervals with thermistors installed at 0.02, 0.05, 0.10, 0.20, and 0.30 m in two locations. Every 2 weeks soil water content was measured with time domain reflectmetry (TDR) probes at 0.05, 0.10, 0.20, and 0.30 m in the same two locations as the thermistors, and snowpack depths were determined with measuring sticks at 10 locations in each of three sites. Half-hourly data for solar radiation, air temperature, humidity, wind speed and precipitation were recorded continuously within 2 km of the experimental site.

The ecosystem simulation model *ecosys* was initialized by allocating organic C in each soil layer of the Dalhousie clay loam (Table 3 with upper layers subdivided to improve model resolution) to active and passive substrate-microbe complexes in a ratio of 1.0:1.5. Estimates of surface and subsurface residue from the barley crop harvested at the start of the field experiment were used to initialize the plant residue complex in each soil layer. Small fractions (0.01 – 0.02) of the C in each complex were used to initialize the soluble, sorbed, microbial community and microbial residue components according to equilibrium values observed in earlier modeling experiments. The model was then run with the attributes of the Dalhousie clay loam (Table 3) under hourly surface boundary conditions for solar radiation, air temperature, humidity, wind speed and precipitation reported from the experimental site between 1 September 1995 and 30 April 1996. Biological (equations (1) – (13)) and physical (equations (14) – (21)) processes were solved on time steps of 1 hour and 2 minutes respectively, with surface boundary conditions assumed constant during each hour. Under natural field conditions the distributions of soil C among the different states within each substrate-microbe complex approach equilibrium within 1 month of model initialization.

Model estimates of soil temperature, soil water content and snowpack depth were first compared with measured data to determine the accuracy with which the model simulated the physical environment of the soil profile at the experimental site. Model estimates of surface N_2O and CO_2 fluxes (equation (21)) were then compared with measured fluxes (equation (22)) to test model hypotheses (equations (1) – (20)). Longer-term comparisons between *ecosys* estimates and N_2O flux measurements will be presented in another paper.

4. Results

4.1 Laboratory Experiment

Simulated versus measured results for denitrifier growth yields during exponential growth on an amino acid substrate are given in Table 4. Simulated yields were reduced from their theoretical maxima under ambient and zero atmospheric O_2 concentrations of 6.0 and 3.4 g C mol^{-1} respectively by maintenance respiration and decomposition (equation (13)). The value of f_e in (3) allowed the ratio of maximum growth rates (h^{-1}) simulated during exponential growth under zero versus ambient O_2 to reach 0.15. This ratio was consistent with that of 1/5 to 1/7 reported by *Koike and Hattori* [1975a].

4.2 Field Experiment

Low air temperatures recorded during November 1995 caused soil cooling (Figure 1a) and freezing (indicated by falling soil water content at successively lower depths in Figure 1b) in the model. Winter precipitation caused a snowpack of 300 – 400 mm to be maintained in the model from early December 1995 until late March 1996 (Figure 1c), which was close to that measured. Following snowmelt in late March the soil warmed (Figure 1a) and thawed (Figure 1b) at successively lower depths during April 1996. Freezing of the soil surface in the model during late November 1995 (Figure 1b) caused aqueous O_2 concentrations in the upper 0.1125 m of the soil profile to decline rapidly, reaching near zero values by late December (Figure 1d). Aqueous O_2 concentrations below 0.15 m declined more gradually over the winter because organic C concentrations and hence C oxidation rates were less. These declines occurred because water in the model was drawn upward to the surface during freezing [*Grant*, 1992], causing soil pores to be occupied by water and ice. Consequently gaseous surface transfers of O_2 (equation (20)) were constrained by very low gaseous diffusivity (equation (18)) so that subsurface O_2 transfers (equations (15) and (17)) and uptake (equation (2)) depended more upon aqueous surface transfers of O_2 (equation (19)). These transfers were slow because aqueous diffusivity (equation (16)) was small, so that soil O_2 became depleted especially near the surface where organic C concentration and hence biological activity were greatest. The thawing and drainage of the soil during April 1996 (Figures 1a and 1b) caused air-filled porosity and hence gaseous surface transfers of O_2 to rise, causing aqueous O_2 concentrations to rise as well (Figure 1d).

Concentrations of NO_3^- in the upper 0.20 m of the soil profile (Figures 2a, 2b and 2c) were reduced in the model from initial values (Table 2) following 93 mm of rain on 6 – 7 October 1995 which caused movement of soil water to depths below 0.35 m (Figure 1b). Concentrations of NO_3^- below 0.25 m in the soil profile were increased by the same rainfall (Figure 2d). Concentrations of NO_3^- rose (Figure 2) during soil freezing in late November (Figures 1a and 1b) and then declined gradually in the upper 0.1125 m from December until April (Figures 2a and 2b) when aqueous O_2 concentrations fell (Figure 1d). These declines were driven in the model by NO_3^- reduction (equation (4) that occurred when O_2 uptake by denitrifiers was constrained by low O_2 concentrations (equation (2)). Nitrate reduction caused increases in NO_2^- concentrations (Figures 2a and 2b) and hence in NO_2^- reduction (equation (5)). Rates of NO_2^- reduction were initially constrained by high NO_3^- and low NO_2^- concentrations (equation (5)), so that increases in aqueous N_2O concentrations in the model did not begin until late January 1996 in the upper 0.11 m of the soil (Figures 2a and 2b) and late February 1996 below 0.15 m (Figure 2c). Concentrations of N_2O above 0.20 m increased gradually during the winter and then declined rapidly when soil O_2 concentrations rose during April 1996 (Figure 1d). Maximum N_2O concentrations attained in the model were ~ 5.0 g N m^{-3} above 0.1125 m and ~ 2.0 g N m^{-3} below 0.15 m. Rates of N_2O reduction were initially constrained in the model by high NO_2^- and low N_2O concentrations (equation (6)) so that decreases in aqueous N_2O concentrations did not begin until late March or early April 1996 (Figure 2) after NO_2^- concentrations had declined. Only limited amounts of NO_2^- and N_2O accumulated below 0.25 m (Figure 2d) because anaerobic conditions did not develop (Figure 1d).

A comparison of soil temperatures and water contents simulated and measured during March and April 1996 is given in Figures 3a and 3b. In the model, thawing in the upper 0.075 m of the soil profile started on 30 March (day of year (DOY) 90 in Fig. 3b) just after disappearance of the snowpack (Figure 1c). Thawing was completed on 2 April (DOY 93) when soil temperatures above 0°C were first observed, but diurnal freeze-thaw cycles continued until 18 April (DOY 109) after which soil temperatures above 0°C were sustained (Figure 3a). The timing and duration of thawing in the model were confirmed by the rise in measured temperature to 0°C at the end of March, by diurnal rises in measured temperature above 0°C during early April, and by the maintenance of above-zero temperatures after mid-April (Figure 3a). Thawing of the upper 0.075 m in the model was also confirmed by a rise in measured soil water content in early April (Figure 3b). The TDR probes used in the field experiment may not measure soil water content accurately when the soil is frozen, so that the readings reported for March may be affected. Thawing at 0.075 – 0.1125 m in the model started on 2 April (DOY 93) and was completed on 8 April (DOY 99), as was also confirmed by diurnal rises in measured soil temperatures (Figure 3a) and by increases in soil water contents (Figure 3b). Thawing below 0.15 m started slowly during early April, but was not completed until 18 April (DOY 109) at 0.15 – 0.20 m and on 22 April (DOY 113) at 0.25 – 0.35 m, after which soil temperatures started to rise. Completion of thawing at 0.25 – 0.35 m in the model was 5 days later than that at 0.30 m in the field.

The timing and duration of soil thawing in the model directly affected the timing and intensity of N_2O emissions. These emissions occurred in two episodes, the first from 29 March to 5 April (DOY 89 – 96) and the second from 10 to 16 April (DOY 101 – 107) (Figure 3c). These two episodes co-incided with two periods during which more intense N_2O emissions were measured

Table 4. Denitrifier Growth Yields Simulated and Measured on an Amino Acid Substrate under Ambient and Zero Atmospheric O_2 Concentrations at 30°C[¶]

	Simulated, g C mol^{-1} C	Measured, g C mol^{-1} C
Ambient O_2	5.1	5.8
Zero O_2	2.7	3.0

[¶] Measured data are from *Koike and Hattori* [1975a].

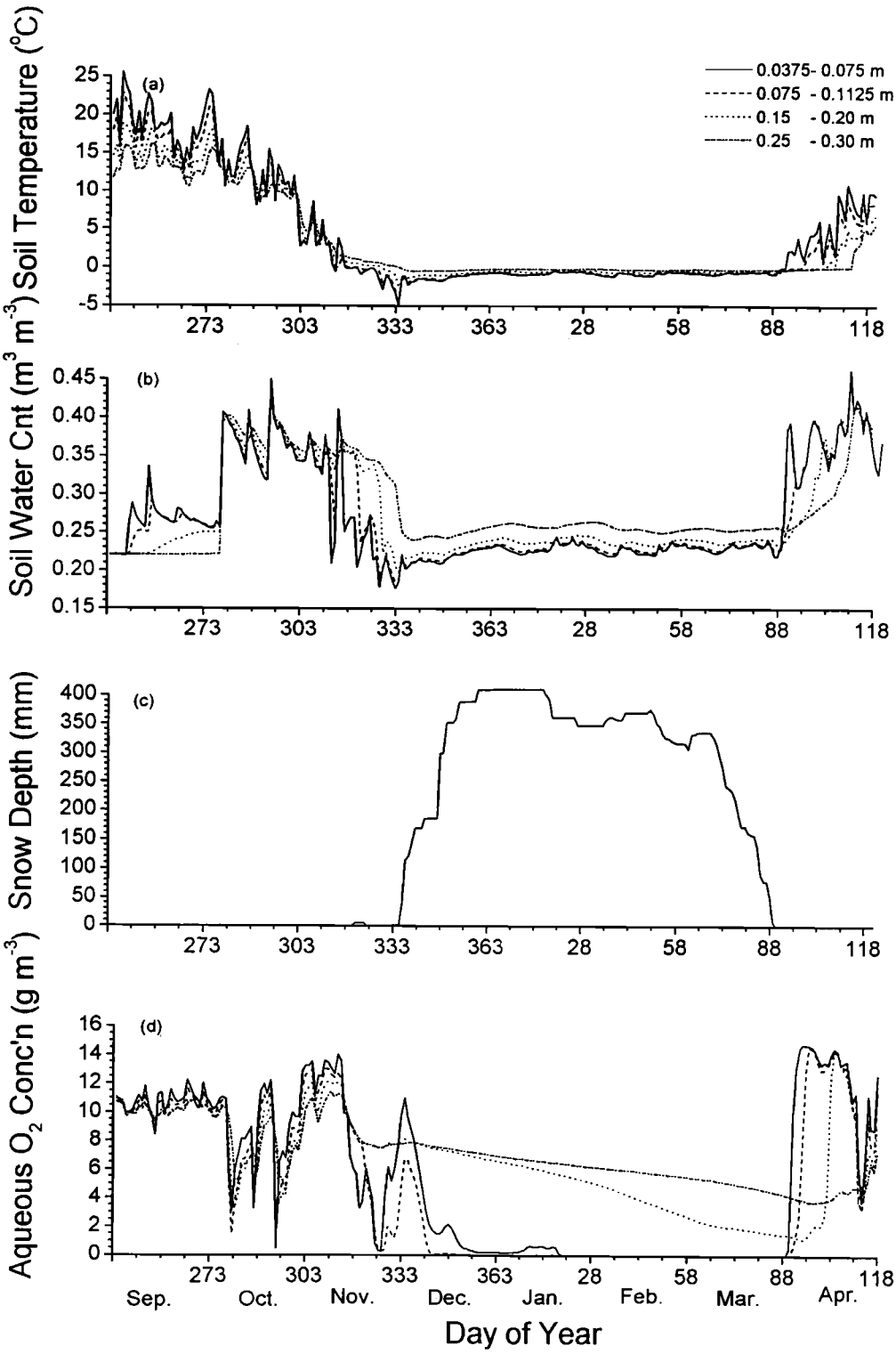

Figure 1. (a) Maximum daily soil temperature, (b) soil water content, (c) snowpack depth and (d) aqueous O_2 concentrations simulated at four different depths from September 1995 to April 1996.

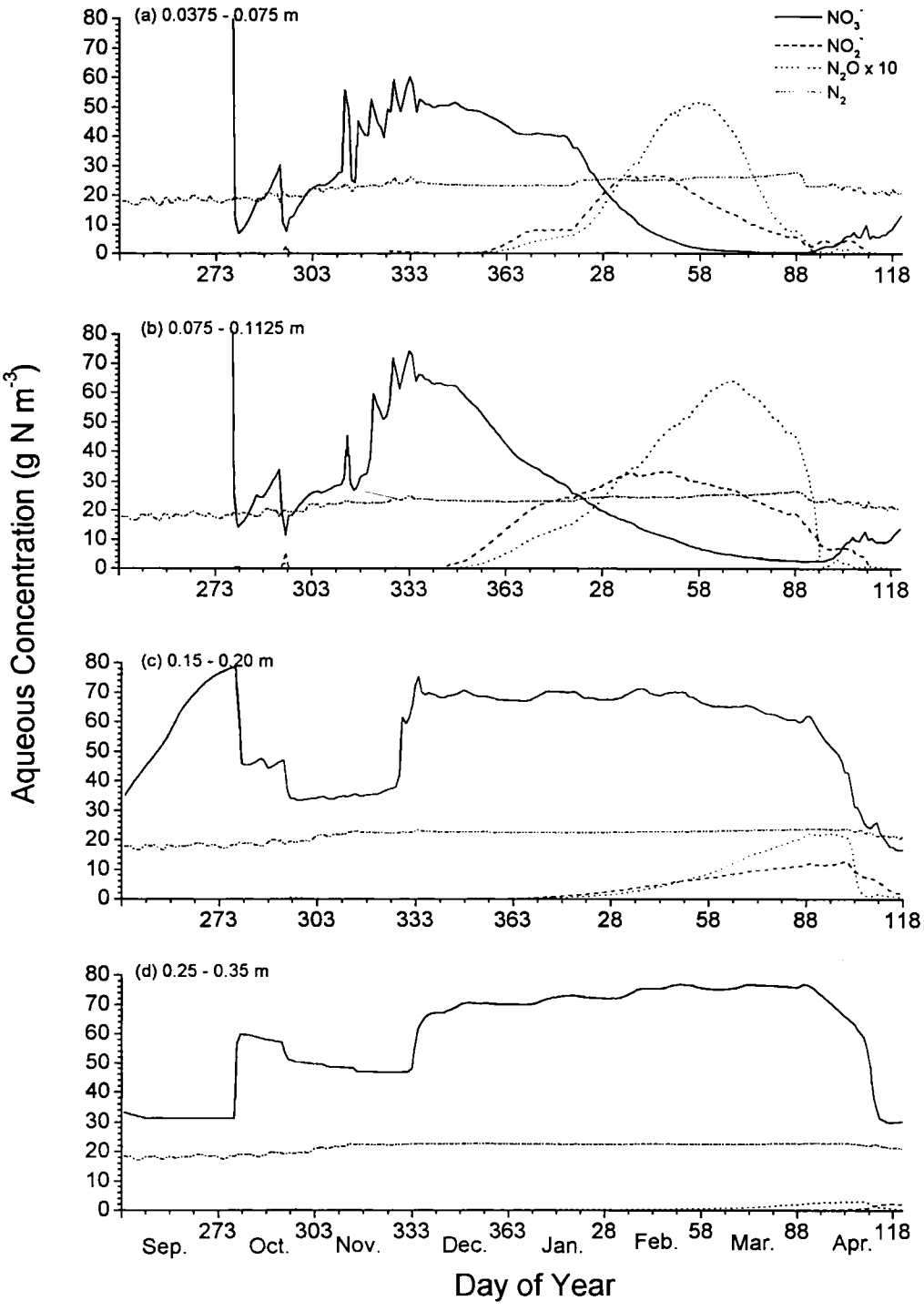

Figure 2. Aqueous concentrations of NO_3^-, NO_2^-, N_2O and N_2 simulated from September 1995 to April 1996 at depths of (a) 0.0375 – 0.075 m, (b) 0.075 – 0.1125 m, (c) 0.15 – 0.20 m and (d) 0.25 – 0.35 m.

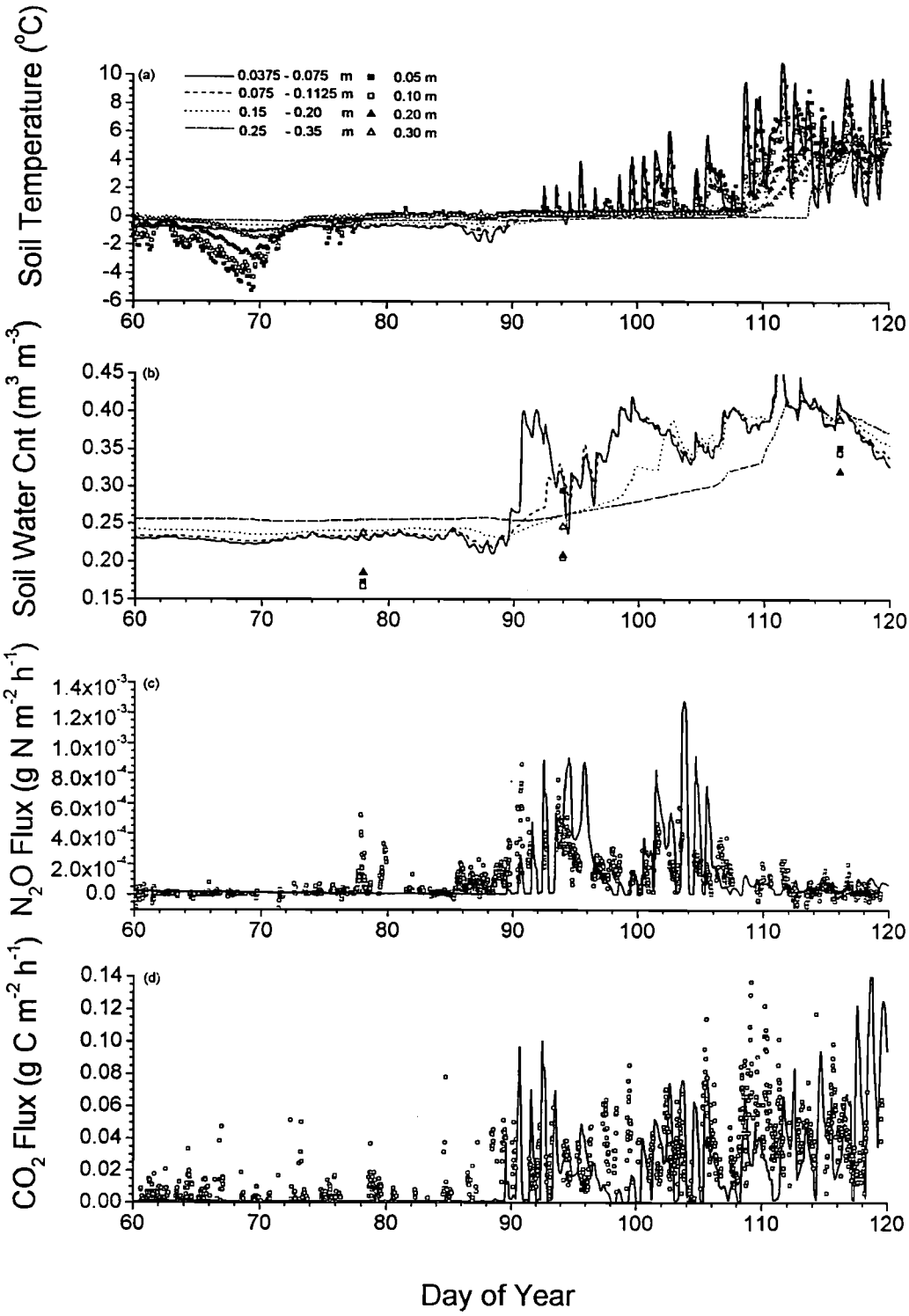

Figure 3. (a) Soil temperatures and (b) soil water contents at four different depths, and (c) surface N_2O and (d) surface CO_2 fluxes simulated (lines) and measured (symbols) during March and April 1996. Measured soil temperatures are plotted every fourth hour. .

in the field. During these episodes emission reached maximum rates of about 1 mg N m^{-2} h^{-1} in both the model and the field. A brief emission episode measured in the field from 18 to 20 March (DOY 78 – 80) was not simulated. Emission rates simulated and measured after 16 April remained low.

In the model, N_2O emission episodes occurred just after drainage events from 1 to 5 April (DOY 92 – 96) that followed soil thawing and from 9 to 15 April (DOY 100 – 106) that followed precipitation (Figure 4a). The episodes were separated by a period of precipitation from 7 to 9 April (DOY 98 – 100) during which emission was suppressed. The drainage events coincided with increases in aqueous concentrations of O_2 (Figure 1d) and declines in those of N_2O (Figure 2). The re-establishment of a gaseous phase during drainage allowed volatilization of aqueous N_2O and other gases (equation (14)) and their rapid transfer in the gaseous phase (equation (17)) to the soil surface where they were emitted (equation (20)). Both volatilization and transfer increased with soil temperature, the former because gaseous solubility declines with temperature ($f_{t_{gsN_2O}}$ in (14)), and the latter because gaseous diffusivity increases with temperature (f_{t_g} in (18)). Soil temperature also controlled gaseous diffusivity at the soil surface (D'_{gN_2O} in (20)) through the effect of diurnal freeze-thaw cycles on water movement and hence air-filled porosity (θ_g in (18)). This control on diffusivity caused emissions in the model to decline rapidly during nights when freezing occurred, to remain low during the following mornings until thawing was completed, and then to rise rapidly during the afternoons as air-filled porosity increased (Figure 4a). Similarly rapid changes were apparent in measured N_2O emissions, although these changes did not always coincide with those simulated.

Simulated CO_2 emissions rose during drainage of the surface soil after thawing (DOY 92 – 96) or precipitation (DOY 100 – 106 and DOY 114 – 120) and were suppressed by rewetting of the surface soil during periods of precipitation (DOY 98 – 100 and DOY 106 – 112) (Figure 3d). Simulated CO_2 emissions were also affected by diurnal freeze-thaw cycles (Figure 4b) as were those of N_2O (Figure 4a). Although the suppression of CO_2 emissions during rewetting of the surface soil was not apparent in the field measurements (Figure 3d), diurnal ranges in measured emissions were similar to those simulated.

5. Discussion

There are two basic criteria used in the selection of model algorithms in *ecosys*. All algorithm parameters required by the model (Table 2) must be capable of evaluation in experiments conducted (1) independently of the model and (2) at spatial and temporal scales smaller than those at which model estimates are to be made. These criteria are deemed necessary to the development of robust, widely applicable models that integrate existing scientific knowledge. These two criteria were used to parameterize basic concepts in microbial biology and soil physics so as to simulate phenomena related to N_2O emissions that have been observed in several independent experiments.

The overwinter increases and early spring decreases in aqueous N_2O concentrations simulated by the model (Figure 2) are consistent in magnitude with increases and decreases in

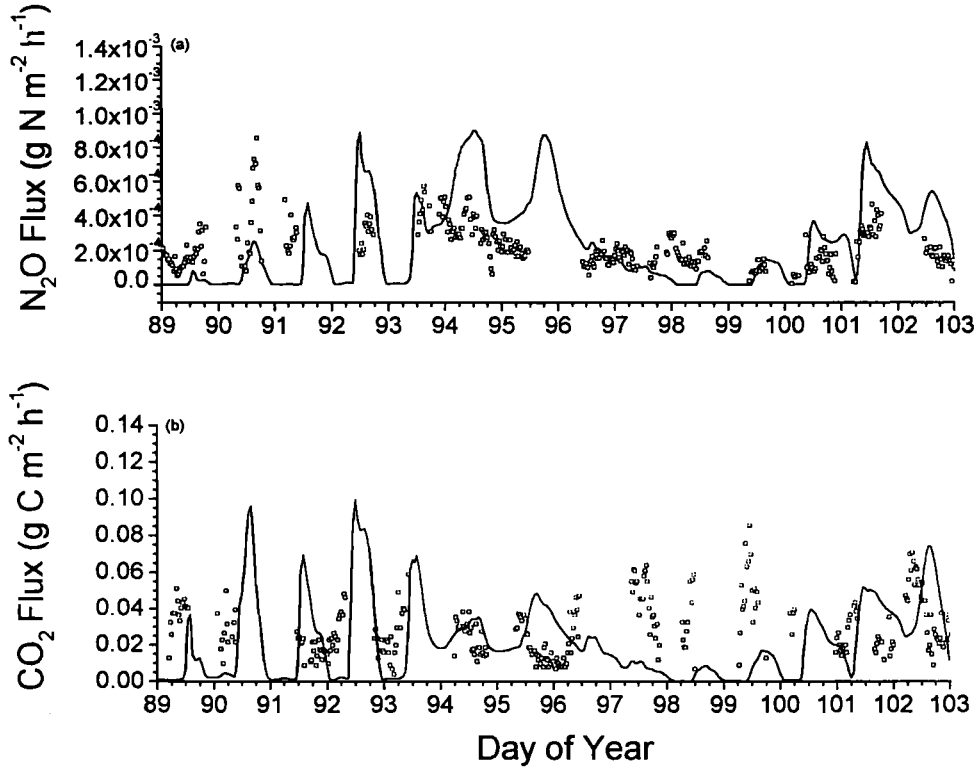

Figure 4. Surface (a) N_2O and (b) CO_2 fluxes simulated (lines) and measured (symbols) from 29 March to 12 April (DOY 89 to 103) 1996.

gaseous N_2O concentrations measured in frozen and thawing soils elsewhere [*Burton and Beauchamp*, 1994; *Cates and Keeney*, 1987; *Flessa et al.*, 1995; *Goodroad and Keeney*, 1984; *Van Bochove et al.*, 1996]. In the model, increases in aqueous N_2O concentrations during winter follow decreases in NO_3^- and increases in NO_2^- concentrations (Figure 2), thereby reproducing the product sequence of denitrification reported by *Cooper and Smith* [1963]. This sequence arises from the hypothesized preference scheme for electron acceptors $O_2 > NO_3^- > NO_2^- > N_2O$ represented in equations (4), (5) and (6) in which the reduction of acceptors with a higher oxidation number suppresses the reduction of those with a lower one.

The coupling of this preference scheme with a physically based treatment of heat and water transport through soils allowed the model to reproduce approximately the timing and intensity of N_2O emissions during spring thaw (Figure 3c). These emissions were driven by C oxidation rates that were similar in magnitude to those measured (Figure 3d), indicating that the coupling of electron donors and acceptors in the model (equations (3) – (9)) was realistic. The episodic nature of N_2O emissions and their association with soil thawing has also been observed by *Christensen and Tiedje* [1990], *Flessa et al.* [1995], *Goodroad and Keeney* [1984] and *Nyborg et al.* [1997]. The temporal distribution of these emissions in the model was strongly controlled by formation and melting of ice layers in the soil which impeded gas exchange with the atmosphere, as has been observed experimentally by *Burton and Beauchamp* [1994]. The accuracy of gaseous fluxes simulated in frozen soils therefore depends upon the extent to which the gaseous phase is reduced by ice formation. Because water migrates towards zones of freezing in *ecosys*, ice eventually occupies most of the non–water–filled porosity of frozen soil if enough water is present in unfrozen soil below, and so impedes gaseous transfer. The modeling work presented here thus contributes to the need indentified by *Frolking et al.* [1998] for models of N_2O emission to simulate soil water dynamics, including freeze–thaw cycles, and to link these dynamics to denitrification activity.

The large diurnal variation of N_2O emissions in the model (Figures 3c and 4a) is consistent with that measured here and elsewhere [*Blackmer et al.*, 1982; *Christensen*, 1983; *Robertson*, 1994), and indicates the importance of temperature-sensitive hydrologic controls on these emissions. Such variation complicates efforts to make temporally integrated estimates of N_2O emissions from discontinuous flux measurements. The ability of simulation models to reproduce this variation is therefore an important test of their capability to make such estimates. It may be argued that if N_2O emissions during spring thaw are driven by denitrification products accumulated under ice during the previous winter (Figure 2), then annual estimates of these emissions need only be based on estimates of total winter denitrification. However these estimates would still require a knowledge of annual freeze-thaw cycles and the kinetics of the denitrification reaction sequence, both of which may be highly variable under site–specific conditions. For example, a mid–January thaw at the field site would, according to the model, cause only small emissions of N_2O (Figure 2), as has been observed elsewhere in January after several weeks of soil freezing [*Christensen and Tiedje*, 1990]. However, reoxygenation of the soil profile during the thaw would cause the oxidation of NO_2^- to NO_3^- [*Grant*, 1994], so that with the resumption of anaerobic conditions after refreezing the reduction of NO_3^- to NO_2^- would have to continue for some time before N_2O would start to accumulate again. This delay in accumulation would cause spring emissions to be much lower than without the January thaw. Such a delay might explain the lower N_2O emission rates reported from successive thawing events by *Flessa et al.* [1995]. Conversely a soil with more rapid rates of C oxidation than those recorded at the field site, caused perhaps by heavy fertilizer or manure applications, would generate a more intense demand for electron acceptors that under anaerobic conditions would cause the N reduction sequence to be accelerated. Such a soil would yield greater N_2O emissions from a mid–winter thaw than those hypothesized here [e.g. *Flessa et al.*, 1995], but under prolonged freezing might yield very little because the reduction sequence would be forced to completion as N_2. It therefore appears unlikely that N_2O emissions can be modeled as simple functions of soil temperature or water content.

The ecosystem model *ecosys* simulates microbial oxidation-reduction reactions under different soil amendments such as crop residue [*Grant et al.*, 1993a], fertilizer [*Grant*, 1993d; *Grant*, 1995] or manure, and under different soil management practices such as rotation and tillage [*Grant*, 1997; *Grant et al.*, 1995; *Grant and Rochette*, 1994] or irrigation. By coupling these reactions to aqueous and gaseous transport of reactants and products, *ecosys* enables the effects of different amendments and managements on N_2O emissions to be estimated. These estimates should recognize that emissions are controlled by spatial variability in substrate concentrations at two scales of resolution: (1) small scale (1 – 10 m) variability due to past C inputs and (2) larger scale (10 – 100 m) variability due to topographic position (slope, aspect, elevation). The first scale is recognized to a limited extent in *ecosys* by calculating oxidation–reduction reactions separately for each organic substrate. For example, a small soil zone with a large concentration of easily decomposable plant residue ($i = y$) (often called a "hot spot") would generate a large demand for electron acceptors ($R'_{y,h}$ in (1)) and hence O_2 ($R'_{o_2 y,h}$ in (2)). This demand, coupled to constraints imposed upon O_2 transfer within the soil zone by dissolution (T_{o_2} in (14)) and diffusion ($D_{s_{O_2}}$ in (2)) would increase the demand for alternative electron acceptors by denitrifiers (R_e in (4) – (6)) and hence the reduction of N. The demand for electron acceptors generated by other organic substrates within the same soil zone ($i \neq y$) would not be affected by the demand generated by the plant residue, and the demand for alternative electron acceptors by denitrifiers would be only indirectly affected through increased competition for O_2. The second scale of spatial variability is recognized in *ecosys* by representing landscapes as grids of north-south columns and east-west rows with defined soil properties (e.g. Table 3) and defined slopes and aspects from which relative elevations are computed. These slopes, aspects and elevations are used in the calculation of heat, water, solute and gas fluxes in three dimensions through the simulated landscape. This representation of spatial variability has been used with the model for N_2O emissions described above to demonstrate that the majority of N_2O emissions from complex landscapes originate from lower slope positions (R.F. Grant, unpublished data, 1997), as has been measured experimentally. Further research at the landcape scale is needed to test *ecosys* and other ecosystem models in order to improve confidence in model estimates of landscape-level emissions of N_2O. These estimates could then be used to arrive at regional estimates of N_2O emissions.

Notation[1]

A_{gs} air-water interfacial area in soil ($m^2\ m^{-2}$) (14).

$D_{g\gamma}$ gaseous diffusivity of gaseous substrate or product γ in soil ($m^2\ h^{-1}$) (17),(18) and (20).

$D'g_{g\gamma}$ gaseous diffusivity of gaseous substrate or product γ in water at 30°C ($m^2\ h^{-1}$) (18).

$D_{i,h,j,c}$ decomposition of heterotrophs (g C $m^{-2}\ h^{-1}$) (13).

$D_{s_{O_2}}$ aqueous dispersivity-diffusivity of O_2 in soil ($m^2\ h^{-1}$) (2).

$D_{s\gamma}$ aqueous dispersivity-diffusivity of substrate or product γ in soil ($m^2\ h^{-1}$) (15), (16) and (19).

$D'_{s\gamma}$ aqueous diffusivity of substrate or product γ in water at 30°C ($m^2\ h^{-1}$) (16).

$D_{t\gamma}$ volatilization-dissolution transfer coefficient (m h^{-1}) (14).

d_m radius of heterotrophic microsite (m) (2).

d_w radius of d_m + water film at current water content (m) (2).

F_j partitioning coefficient for j in $M_{i,h,j}$ (13).

f_e fraction of electrons not accepted by O_2 transferred by denitrifiers to N oxides (3).

f_t temperature function for microbial processes (dimensionless) (1).

f_{t_g} temperature function for gaseous diffusivity (dimensionless) (18).

$f_{t_{gs}\gamma}$ temperature function for solubility of gaseous substrate or product γ (dimensionless) (14) and (19).

f_{t_a} temperature function for aqueous diffusivity (dimensionless) (16).

f_w water stress function for microbial processes (dimensionless) (1).

ΔG_d free energy change of heterotrophic C oxidation - N reduction (kJ g C^{-1}) (12).

ΔG_h free energy change of heterotrophic C oxidation - O_2 reduction (kJ g C^{-1}) (12).

G_M energy required to construct new M from $P_{i,k}$ (kJ g C^{-1}) (12)

g_a boundary layer conductance between the atmosphere and the soil surface (h m^{-1}) (19).

$[\gamma_a]$ concentration of gaseous substrate or product γ in the atmosphere (g m^{-3}) (19) and (20).

$[\gamma_g]$ concentration of gaseous substrate or product γ in the gaseous phase of the soil (g m^{-3}) (14), (17) and (20).

$[\gamma_s]$ concentration of substrate or product γ in the aqueous phase of the soil (g m^{-3}) (14), (15) and (19).

$K_{NO_2^-d}$ M-M constant for reduction of NO_2^- by heterotrophic denitrifiers (g N m^{-3}) (5).

$K_{NO_3^-d}$ M-M constant for reduction of NO_3^- by heterotrophic denitrifiers (g N m^{-3}) (4).

K_{N_2Od} M-M constant for reduction of N_2O by heterotrophic denitrifiers (g N m^{-3}) (6).

K_{O_2h} M-M constant for reduction of O_{2S} by heterotrophs (g $O_2\ m^{-3}$) (2).

K_{Rh} M-M constant for respiration of $P_{i,c}$ by heterotrophs (g C m^{-3}) (1).

λ hydrodynamic dispersion coefficient (m) (16).

$M_{i,h,a}$ active biomass of heterotrophs (g C m^{-2}) (1) and (2).

$M_{i,h,j,c}$ biomass of heterotrophs (g C m^{-2}) (13).

$[NO_2^-]$ concentration of NO_2^- in soil solution (g N m^{-3}) (5).

$[NO_3^-]$ concentration of NO_3^- in soil solution (g N m^{-3}) (4).

$[N_2O]$ concentration of N_2O in soil solution (g N m^{-3}) (6).

n number of active heterotrophic microsites (g^{-1}) (2).

$[O_{2m}]$ O_2 concentration at heterotrophic microsites (g $O_2\ m^{-3}$) (2).

$[O_{2S}]$ O_2 concentration in soil solution (g $O_2\ m^{-3}$) (2).

$[P_{i,c}]$ concentration of soluble decomposition products of $S_{i,c}$ in soil solution (g C m^{-3}) (1).

$Q'_{g\gamma}$ vertical transport of gaseous substrate or product γ between the atmosphere and the soil surface (g $m^{-2}\ h^{-1}$) (21).

$Q_{g\gamma}$ vertical transport of gaseous substrate or product γ in the gaseous phase of the soil (g $m^{-2}\ h^{-1}$) (17).

$Q'_{g\gamma}$ vertical transport of gaseous substrate or product γ between the atmosphere and the gaseous phase of the soil surface (g $m^{-2}\ h^{-1}$) (20) and (21).

$Q_{s\gamma}$ vertical transport of substrate or product γ in the aqueous phase of the soil (g m^{-2} h^{-1}) (15).

$Q'_{s\gamma}$ vertical transport of substrate or product γ between the atmosphere and the aqueous phase of the soil surface (g m^{-2} h^{-1}) (19) and (21).

Q_w vertical transport of water (m^3 m^{-2} h^{-1}) (15), (16) and (17).

θ_g soil air content (m^3 m^{-3}) (18).

θ_p soil porosity (m^3 m^{-3}) (18).

θ_s soil water content (m^3 m^{-3}) (16).

R_e electron transfer to N oxides by denitrifiers (mol e^- m^{-2} h^{-1}) (3), (4), (5) and (6).

R'_h specific oxidation of $P_{i,c}$ by heterotrophs at saturating $[P_{i,c}]$, 30°C and high water potential (g C g C^{-1} h^{-1}) (1).

$R_{i,d}$ oxidation of $P_{i,c}$ coupled to reduction of N by denitrifiers (g C m^{-2} h^{-1}) (8), (9) and (11).

$R_{i,h}$ oxidation of $P_{i,c}$ coupled to reduction of O_2 by heterotrophs under ambient $[O_{2S}]$ (g C m^{-2} h^{-1}) (7), (9) – (11) and (13).

$R'_{i,h}$ oxidation of $P_{i,c}$ coupled to reduction of O_2 by heterotrophs under saturating $[O_{2S}]$ (g C m^{-2} h^{-1}) (1) and (7).

$R_{Mi,h}$ maintenance respiration by heterotrophs (g C m^{-2} h^{-1}) (10), (11) and (13).

$R_{NO_2 i,d}$ NO_2^- reduction by heterotrophic denitrifiers (g N m^{-2} h^{-1}) (5), (6) and (8).

$R_{NO_3 i,d}$ NO_3^- reduction by heterotrophic denitrifiers (g N m^{-2} h^{-1}) (4), (5), (6) and (8).

$R_{N_2 Oi,d}$ N_2O reduction by heterotrophic denitrifiers (g N m^{-2} h^{-1}) (6) and (8).

$R_{O_2 i,h}$ O_2 reduction by heterotrophs under ambient $[O_{2S}]$ (g O_2 m^{-2} h^{-1}) (2), (3) and (7).

$R'_{O_2 i,h}$ O_2 reduction by heterotrophs under saturating $[O_{2S}]$ (g O_2 m^{-2} h^{-1}) (2), (3) and (7).

S_γ Ostwald solubility coefficient of gaseous substrate or product γ at 30°C (14) and (19).

T_γ exchange of gaseous substrate or product γ between gaseous and aqueous phases in the soil (g m^{-2} h^{-1}) (14).

τ_s tortuosity coefficient for aqueous diffusion (16).

$U_{i,h,c}$ $P_{i,c}$ uptake by $M_{i,h}$ (g C m^{-2} h^{-1}) (10), (11) and (13).

U_w root uptake of water (m^3 m^{-2} h^{-1}) (17).

υ_g sensitivity of τ_g to θ_g (18).

υ_s sensitivity of τ_s to θ_s (16).

Y_d biomass yield from heterotrophic reduction of N (g M g C^{-1}) (11) and (12).

Y_h biomass yield from heterotrophic reduction of O_2 (g M g C^{-1}) (10) and (12).

z depth to mid-point of soil layer (m) (15), (17), (19) and (20).

[¶] numbers in parentheses indicate equation(s) in which variable is used.

Acknowledgements. This research is part of the Global Change and Terrestrial Ecosystems project of the International Geosphere-Biosphere Programme. It was conducted with the support of Agriculture and Agri-Food Canada, PERD program. We are grateful to Dave Dow and Mark Edwards for their excellent technical assistance.

References

Allison, F.E., S.N. Carter and L.D. Sterling, The effect of partial pressure of oxygen on denitrification in soil, *Soil Sci. Soc. Am Proc. 24*, 283-285, 1960.

Ameida, J.S., M.A.M. Reis, and M.J.T. Carrondo, Competition between nitrate and nitrite reduction in denitrification by *Pseudomonas fluorescans*, *Biotechnol. Bioeng., 46*, 476-484, 1995.

Arah, J.R.M., and A.J.A. Vinten, Simplified models of anoxia and denitrification in aggregated and simple-structured soils, *Eur. J. Soil Sci., 46*, 507-517, 1995.

Betlach, M.R., Accumulation of intermediates during denitrification - Kinetic mechanisms and regulation of assimilatory nitrate uptake, Ph.D. thesis, Mich. State Univ., East Lansing, *Diss. Abstr.* 80:06083, 1979.

Blackmer, A.M., and J.M. Bremner, Inhibitory effect of nitrate on reduction of N_2O to N_2 by soil microorganisms, *Soil Biol. Biochem., 10*, 187-191, 1978.

Blackmer, A.M., S.G. Robbins, and J.M. Bremner, Diurnal variability in rate of emission of nitrous oxide from soils, *Soil Sci. Soc. Am. J., 46*, 937-942, 1982.

Bremner, J.M., and K. Shaw, Denitrification in soils, II, Factors affecting denitrification, *J. Agric. Sci., 51*, 40-52, 1958.

Bresler, E., Simultaneous transport of solutes and water under transient unsaturated flow conditions, *Water Resour. Res., 9*, 975-986, 1973.

Burton, D.L.. and E.G. Beauchamp, Profile nitrous oxide and carbon dioxide concentrations in a soil subject to freezing. *Soil Sci. Soc. Am. J., 58*, 116-122, 1994.

Cady, F.B., and W.V. Bartholomew, Influence of low pO_2 on denitrification processes and products, *Soil Sci. Soc. Am. Proc., 25*, 362-365, 1961.

Campbell, G.S., *Soil Physics with BASIC*, 185 pp., Elsevier, New York, 1985.

Cates, R.L.,Jr., and D.R. Keeney, Nitrous oxide production throughout the year from fertilized and manured maize fields, *J. Environ. Qual., 16*, 443-447, 1987.

Christensen, S., Nitrous oxide emission from a soil under permanent grass: seasonal and diurnal fluctuations as influenced by manuring and fertilization, *Soil Biol. Biochem., 15*, 531-536, 1983.

Christensen, S., and J.M. Tiedje, Brief and vigorous N_2O production by soil at spring thaw, *J. Soil Sci., 41*, 1-4, 1990.

Cooper, G.S., and R.L. Smith, Sequence of products formed during denitrification in some diverse western soils, *Soil Sci. Soc. Am. Proc., 27*, 659-662, 1963.

Elliott, R.G., and C.M. Gilmour, Growth of *Pseudomonas stutzeri* with nitrate and oxygen as terminal electron acceptors, *Soil Biol. Biochem., 3*, 331-335, 1971.

Firestone, M.K., M.S. Smith, R.B. Firestone, and J.M. Tiedje, The influence of nitrate, nitrite and oxygen on the composition of the gaseous products of denitrification in soil, *Soil Sci. Soc. Am. J., 43*, 1140-1144, 1979.

Flessa, H., P. Dörsch, and F. Beese, Seasonal variation of N_2O and CH_4 fluxes in differently managed arable soils in southern Germany, *J. Geophys. Res., 100*, 23115-23124, 1995.

Frolking, S.E., et al., Comparison of N_2O emissions from soils at three temperate agricultural sites: simulations of year-round measurements by four models, *Nutr. Cycling. Agroecosyst.*, in press, 1998.

Goodroad, L.L., and D.R. Keeney, Nitrous oxide emissions from soils during thawing, *Can. J. Soil Sci., 64*, 187-194, 1984.

Grant, R.F., Dynamic simulation of phase changes in snowpacks and soils, *Soil Sci. Soc. Am. J., 56*, 1051-1062, 1992.

Grant, R.F., Simulation of ecological controls on nitrification, *Soil Biol. Biochem., 26*, 305-315, 1994.

Grant, R.F., Mathematical modelling of nitrous oxide evolution during nitrification, *Soil Biol. Biochem., 27*, 1117-1125, 1995.

Grant, R.F., *ecosys. Global Change and Terrestrial Ecosystems Task 3.3.1 Soil Organic Matter Network (SOMNET): 1996 Model and Experimental Metadata.*, pp. 19-24, Nat. Environ. Res. Counc. Cent. for Ecol. and Hydrol., Wallingford, Oxon, England, 1996.

Grant, R.F., Changes in soil organic matter under different tillage and rotation: Mathematical modelling in *ecosys*, *Soil Sci. Soc. Am. J., 61*, 752-764, 1997.

Grant, R.F., Mathematical modelling of methanogenesis in *ecosys*, *Soil Biol. Biochem., 30*, 883-896, 1998.

Grant, R.F., Mathematical modelling of methanotrophy in *ecosys*, *Soil Biol. Biochem.*, 31: 287-297, 1999.

Grant, R.F., and P. Rochette, Soil microbial respiration at different temperatures and water potentials: Theory and mathematical modelling, *Soil Sci. Soc Am. J., 58*, 1681-1690, 1994.

Grant, R.F., R.C. Izaurralde, and D.S. Chanasyk, Soil temperature under different surface managements: testing a simulation model, *Agric. For. Meteorol., 73*, 89-113, 1995.

Grant, R.F., N.G. Juma, and W.B. McGill, Simulation of carbon and nitrogen transformations in soils, I, Mineralization, *Soil Biol. Biochem., 27*, 1317-1329, 1993a.

Grant, R.F., N.G. Juma, and W.B. McGill, Simulation of carbon and nitrogen transformations in soils, II, Microbial biomass and metabolic products, *Soil Biol. Biochem., 27*, 1331-1338, 1993b.

Grant, R.F., M. Nyborg, and J. Laidlaw, Evolution of nitrous oxide from soil, I, Model development, *Soil Sci., 156*, 259-265, 1993c.

Grant, R.F., M. Nyborg, and J. Laidlaw, Evolution of nitrous oxide from soil, II, Experimental results and model testing, *Soil Sci., 156*, 266-277, 1993d.

Griffin, D.M., *Ecology of Soil Fungi*, 193 pp., Syracuse Univ. Press, Syracuse N.Y., 1972.

Horst, T.W., and J.C. Weil, How far is far enough? The fetch requirements for micrometeorological measurement of surface fluxes, *J. Atmos. Oceanic Technol., 11*, 1018-1025, 1994.

Kemper, W.D., and J.B. Rollins, Osmotic efficiency coefficients across compacted clays, *Soil Sci. Soc.Amer. Proc., 30*, 529-534, 1966.

Koike, I., and A. Hattori, Growth yield of a denitrifying bacterium, *Pseudomonas denitrificans*, under aerobic and denitrifying conditions, *J. Gen. Microbiol., 88*, 1-10, 1975a.

Koike, I., and A. Hattori, Energy yield of denitrification: An estimate from growth yield in continuous cultures of *Pseudomonas denitrificans* under nitrate-, nitrite- and nitrous oxide-limited conditions, *J. Gen. Microbiol., 88*, 11-19, 1975b.

Leffelaar, P.A., and W.W. Wessel, Denitrification in a homogeneous, closed system: experiment and simulation, *Soil Sci., 146*, 335-349, 1988.

Li, C., S. Frolking, and T.A. Frolking, A model of nitrous oxide evolution driven by rainfall events, I, Model structure and sensitivity, *J. Geophys. Res., 97*, 9759-9776, 1992.

McConnaughey, P.K., and D.R. Bouldin, Transient microsite models of denitrification, I, Model development, *Soil Sci. Soc. Am. J., 49*, 886-891, 1985.

McGill, W.B., H.W. Hunt, R.G.Woodmansee, and J.O. Reuss, Phoenix, a model of the dynamics of carbon and nitrogen in grassland soils, in *Terrestrial Nitrogen Cycles*, edited by F.E. Clark and T. Rosswall, *Ecol. Bull., 33*, 49-115, 1981.

Millington, R.J., Gas difusion in porous media, *Science, 130*, 100-102, 1959.

Nommik, H. Investigations on denitrification, *Acta Agric. Scand., 6*, 195-228, 1956.

Nyborg, M., J.W. Laidlaw, E.D. Solberg, and S.S. Malhi, Denitrification and nitrous oxide emissions from a Black Chernozemic soil during Spring thaw in Alberta, *Can. J. Soil Sci., 77*, 153-160, 1997.

Ogram, G.L., F.J. Northrup, and G.C. Edwards, Fast time response tunable diode laser measurements of atmospheric trace gases for eddy correlation, *J. Atm. Oceanic Tech., 5(4)*, 521-527, 1988.

Parton, W.J., A.R. Mosier, D.S. Ojima, D.W. Valentine, D.S. Schimel, K. Weier, and A.E. Kulmala, Generalized model for N_2 and N_2O production from nitrification and denitrification, *Global Biogeochem. Cycles, 10*, 401-412, 1996.

Pattey, E., W.G. Royds, R.L. Desjardins, D.J. Buckley, and P.

Rochette, Software description of a data acquisition and control system for measuring trace gas and energy fluxes by eddy-accumulation and correlation techniques, *Comput. Electron. Agric., 15(4)*, 303-321, 1996.

Paulson, C.A., The mathematical representation of wind speed and profile temperatures in the unstable atmospheric surface layer, *J. Appl. Meteorol., 9*, 857-861, 1970.

Pirt, S.J., *Principles of Microbe and Cell Cultivation*, 274 pp., Blackwell Sci., Cambridge, Mass, 1975.

Ridge, E.H., Studies on soil fumigation, II, Effects on bacteria, *Soil Biol. Biochem., 8*, 249-253, 1976.

Robertson, K., Nitrous oxide emission in relation to soil factors at low to intermediate moisture levels, *J. Environ. Qual., 23*, 805-809, 1994.

Shields, J.A., E.A. Paul, and W.E. Lowe, Factors influencing the stability of labelled microbial materials in soils. *Soil Biol. Biochem., 6*, 31-37, 1974.

Simpson, I.J., G.W. Thurtell, H.H. Neumann, G. den Hartog, and G.C. Edwards, The validity of similarity theory in the roughness sublayer above forests. *Boundary Layer Meteorol.*, in press, 1998.

Skopp J., Oxygen uptake and transfer in soils: analysis of the air-water interfacial area, *Soil Sci. Soc Am. J., 49*, 1327-1331, 1985.

Smid, A.E., and E.G. Beauchamp, Effects of temperature and organic matter on denitrification in soil, *Can. J. Soil Sci., 56*, 385-391, 1976.

Van Bochove, E., H.G. Jones, F. Pelletier, and D. Prévost, Emission of N_2O from agricultural soil under snow cover: a significant part of N budget, *Hydrol. Proc., 10*, 1545-1549, 1996.

Wagner-Riddle, C., G.W. Thurtell, G.E. Kidd, G.C. Edwards, and I.J. Simpson, Micometeorological measurements of trace gas fluxes from agricultural and natural ecosystems, *Infrared Phys. Technol. 37*, 51-58. 1996,

Weier, K.L., J.W. Doran, J.F. Power, and D.T. Walters, Denitrification and the dinitrogen/nitrous oxide ratio as affected by soil water, available C and nitrate, *Soil Sci. Soc. Am. J., 57*, 66-72, 1993.

Wienhold, F.G., H. Frahm, and G.W. Harris, Measurements of N_2O fluxes from fertilized grassland using a fast response tunable diode laser spectrometer, *J. Geophys. Res., 99*, 16557-16567, 1994.

Wilhelm, E., R. Battino, and R.J. Wilcock, Low-pressure solubility of gases in liquid water, *Chem. Rev., 77*, 219-262, 1977.

Yoshinari, T., R. Hynes, and R. Knowles, Acetylene inhibition of nitrous oxide reduction and measurement of denitrification and nitrogen fixation in soil, *Soil Biol. Biochem., 9*, 177-183, 1977.

R. Grant, Department of Renewable Resources, University of Alberta, 442 Earth Sciences Building, Edmonton, Alberta, T6G 2H1, Canada. (robert.grant@ualberta.ca)

(Received May 20, 1998; revised October 19, 1998; accepted November 17, 1998.)